Letter

Structure and pressure dependence of the Fermi surface of lithium

Tushar Bhowmick,[1] Sabri F. Elatresh,[2,*,†] Audrey D. Grockowiak,[3,*] William Coniglio,[3] Mohammad Tomal Hossain,[1] Elisabeth J. Nicol,[4] Stanley W. Tozer,[3] Stanimir A. Bonev,[5,‡] and Shanti Deemyad[1,§]

[1]*Department of Physics and Astronomy, University of Utah, Salt Lake City, Utah 84112, USA*

[2]*Physics Department, King Fahd University of Petroleum and Minerals, Dhahran 31261, Saudi Arabia*

[3]*National High Magnetic Field Laboratory and Department of Physics, Florida State University, Tallahassee, Florida 32310, USA*

[4]*Department of Physics, University of Guelph, Guelph, Ontario, Canada N1G 2W1*

[5]*Lawrence Livermore National Laboratory, Livermore, California 94550, USA*

(Received 1 October 2021; revised 1 April 2022; accepted 9 June 2022; published 18 July 2022)

We report studies of the Fermi surface (FS) of isotopically pure polycrystalline ^{7}Li from ambient pressure to 4.7 GPa. Shubnikov–de Haas (SdH) oscillations at 300 mK in external magnetic fields up to 35 T are measured to map the spherical parts of the FS of lithium. Our ambient pressure data show that the principal SdH frequencies consist of three distinct peaks at 41.25 ± 0.05, 41.65 ± 0.05, and 42.05 ± 0.05 kT, which are theoretically consistent with the presence of two crystal structure domains exhibiting nearly spherical FS. The size of the spherical parts of the FS is compatible with bcc and fcc crystal structures. The measured frequencies at 41.25 and 42.65 kT present direct quantitative evidence for the spherical deformation of the FS in fcc Li. Our high-pressure data show that while the FS of Li deforms under compression, it remains mostly spherical up to 4.7 GPa and the pressure dependence of the SdH frequency is consistent with the theoretically calculated pressure dependence in the fcc structure. Finally, we find that the electron effective mass does not deviate under pressure significantly from its ambient pressure value.

DOI: 10.1103/PhysRevB.106.L041112

While having only three atomic electrons, the electronic and structural properties of solid lithium are quite complex. Lithium is the only monovalent superconducting metal at ambient pressure (P) which breaks Matthias's empirical rule [1,2]. Its phase diagram becomes progressively more complex under P and exhibits a number of symmetry-breaking structural phase transitions, e.g., [3–6] leading to an elemental topological semimetal [7,8], electride phase [9], and anomalous isotope effects within the superconducting state [10]. Unlike most other simple metals, the superconductivity in lithium is enhanced by five orders of magnitude under P, reaching the highest T_c of any element below 100 GPa [11–17]. Many of the nontrivial electronic properties of Li are related to the morphology of its Fermi surface (FS) and its changes under compression [17–22]. Therefore, mapping the FS of Li is central to understanding its complex phase diagram.

A direct way to construct a FS is from measurements of quantum oscillations (QOs) under the application of high magnetic fields. Fermiology experiments at ambient and high P have been carried out on the majority of metallic elements and many other compounds, e.g., [23–29]. Notably, recent fermiology studies on tellurium and black phosphorous have been used to detect their topological electronic states [30,31]. However, despite being the first alkali metal, the only successful studies on Li at low temperature, even at ambient P, were done using an unconventional sample preparation, where small size particles were confined within paraffin wax [32–34]. This unique approach was envisioned in order to suppress the shear-driven partial martensitic transition in Li, since it was thought that the presence of a mixed phase with random crystalline orientations would cause severe phase smearing, which would diminish any observable oscillations at low T. In these early studies, the anisotropy of the bcc structure was calculated by comparing the width of the measured de Haas–van Alphen frequency to the calculated free electron frequency in Li. Other methods, such as positron annihilation, were also used but only to determine the FS of Li above its martensitic transition [35].

Measurements of the FS of Li under P are even more challenging due to anisotropic deformations from nonuniform stress. These deformations and the associated phase smearing cause a spread of the QO frequencies and reduce their amplitude [36]. As such, fermiology studies of Li under P have not been hitherto successful. Moreover, measurements on other alkali metals have only been carried out at P below 0.5 GPa [37].

Here we use advanced fermiology methods in higher and more uniform magnetic fields than previously accessible, accompanied by theoretical calculations, to revisit the experiments in polycrystalline, single-grain, and isotopically pure Li samples. We could observe strong QO and resolve the structural details of the spherical part of the FS of isotopically pure polycrystalline ^{7}Li samples at ambient P. Furthermore,

*These authors contributed equally to this work.
†Corresponding author: sabri.elatresh@kfupm.edu.sa
‡Corresponding author: bonev@llnl.gov
§Corresponding author: deemyad@physics.utah.edu

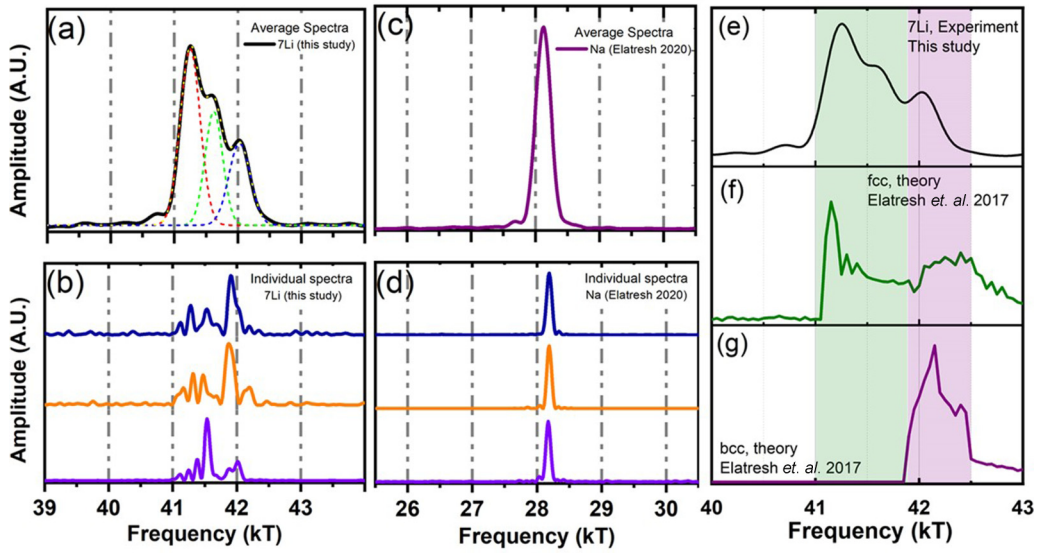

FIG. 1. (a) Average SdH frequency spectrum (solid line) of ^{7}Li data in a 1-T range from measurements at 52 sample orientations. The dotted lines are theoretical fits to the experimental data. (b) ^{7}Li SdH measurements in a 2-T range at a rate 0.30 T/min in three selected orientations. (c) Average of Na SdH data in a 1-T range from measurement at 24 sample orientations. (d) Na SdH measurement in a 2-T range at a rate of 0.30 T/min in three selected orientations. (e)–(g) Comparison of the experimental QO average spectrum of ^{7}Li to the calculated values for bcc and fcc structures [46]. The shaded green and purple regions indicate where the area of the spherical parts of the FS are consistent with theoretically calculated principal frequencies of lithium in the fcc and bcc structures, respectively.

we are able to detect strong QO under pressures exceeding 4.7 GPa.

The presence of impurities, defects, and nonuniform stress can influence the results of fermiology studies, both by suppressing the QO and by affecting the martensitic transitions, which in turn would lead to changes in the FS. To prevent such undesirable effects, isotopically pure polycrystalline samples of ^{7}Li (99.9% isotopically enriched, 99.99% metallic purity from Alfa Aesar) covered with mineral oil were cut and immediately used in our experiments.

To avoid deformations introduced by electrodes, we used a noncontact method with a contactless LC resonant tank circuit driven by tunnel diode oscillators (TDOs) [38,39]. Ambient P data were collected in a ^{3}He superconducting magnet at a base temperature of 360 mK up to 18 T. Additional data were also collected in a dilution refrigerator at a base temperature of 20 mK at magnetic fields up to 16 T.

At ambient P, we can distinguish three distinct Shubnikov–de Haas (SdH) peaks near $\sim$42 kT. To eliminate the possibility of experimental errors such as a field anisotropy leading to slight shifts in the peak positions under various angles, we performed simultaneous calibration experiments on sodium samples which were prepared using identical methods [40] (Fig. 1). Na has the most spherical FS and is an ideal system for calibration [40,41]. Therefore, if the peak splitting were an experimental artifact, we expect to observe them in Na as well. The SdH oscillation frequency spectrum of Na only exhibits one principal peak at 28.1 kT. The shift in frequency of SdH oscillations originating from different orientations is minimal [Fig. 1(d)] and the full width at half maximum for Na is 0.3 kT. This comparison confirms that the observed splitting in Li is an intrinsic property of the sample FS.

Both Li and Na undergo partial martensitic transitions upon cooling. However, while the transition from bcc Li at ambient P is nearly complete by 10 K (75–90%) and it becomes entirely martensite at 4.2 K [33,42,43], the maximum martensite portion in Na does not exceed 43% [43–45]. The structure of martensite Li based on available diffraction pattern data is closely related to a stacking fault mixture of fcc and hcp known as 9R. However, the x-ray and neutron diffraction measurements are not fully compatible with this structure and recent theoretical analysis of the FS of lithium suggests that 9R is not likely the structure of the martensite phase [46]. Moreover, molecular dynamic simulations generate a structure composed of fcc and hcp domains which fit the crystallography data better than 9R [47]. The Brillouin zones (BZs) of ^{7}Li differ significantly in different crystalline structures and 9R does not exhibit a significant number of peaks close to $\sim$42 kT. However, small gaps in the 9R FS may break down under high fields, leading to the appearance of an unreconstructed FS in this frequency range. Meanwhile, both fcc and bcc have their principal peaks between 40 and 45 kT [46].

A comparison with theoretical calculations of the Li FS for different structures [46] shows that the frequency region where the triple peak is observed (near 42 kT) coincides with the location of the calculated single bcc peak and the double peak coming from the spherical part of the fcc FS [Figs 1(e)–1(g)]. Note that the SdH frequencies are sensitive to the structural parameters (see Fig. S11 of the Supplemental Material [48]) and the theoretical calculations rely on 0-K optimized lattice constants. The spread of frequencies over the measured triple peak is within the corresponding accuracy of the computed lattice parameters. Furthermore, due to the incomplete nature of the martensitic transition and the potential presence of other domains such as hcp, deviations of the location of the observed peaks from those calculated for perfect fcc or bcc are expected. Thus, the comparison suggests

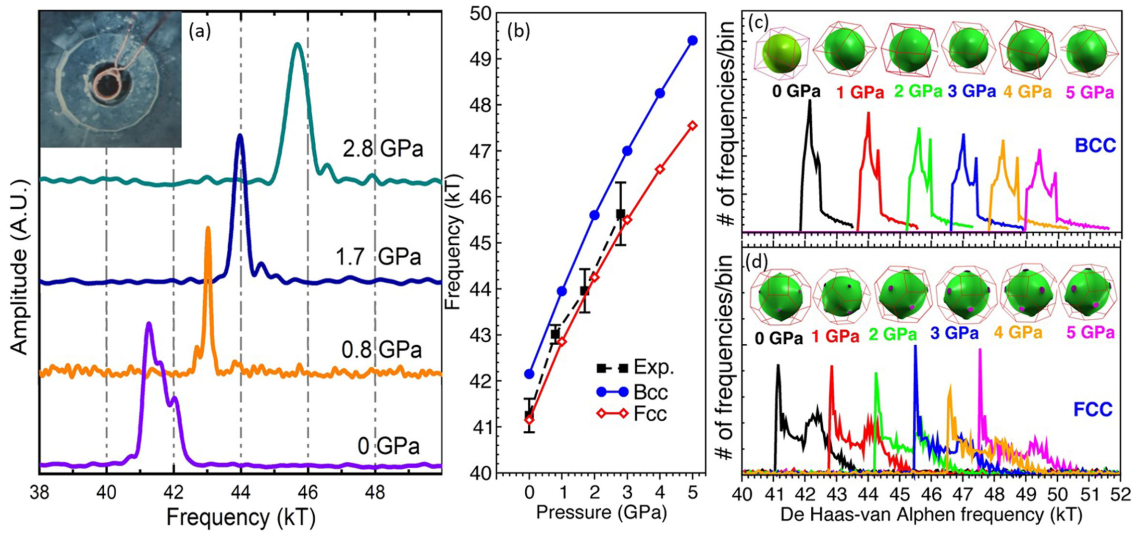

FIG. 2. (a) Average of SdH frequency measurements at different pressures. Here 0-GPa data are the average at a 1-T range and all the others are in the 2-T range. The inset is an image of the coil inside of the DAC for high P measurements. (b) Comparison of the theoretical P dependence of bcc and fcc peaks with the experimental data. (c), (d) Theoretical bcc and fcc QO frequencies for all orientations.

that the measured SdH spectrum can be assigned to a combination of bcc and fcc, but the data do not provide conclusive, quantitative proof. A comparison of the amplitude of the peaks suggests that the majority of the sample is in the fcc phase. It should be noted that the FS of fcc lithium has a neck, which theoretically also produces SdH frequencies around 17 kT [46], however, here experimental evidence for this was only found in two orientations. This is not unexpected, since the necks of the fcc Fermi surfaces are directional and the signal that they produce is low in weight in an orientationally averaged spectra (see Fig. S13 of the Supplemental Material [48]).

Previous fermiology studies on Li have also noted the presence of a potential anisotropy in the radial distortion of its bcc FS, which was not observed in calculations [49]. Due to lack of sufficient resolution, the prior experimental data remained inconclusive as they could not identify the main peaks or resolve the structure of the principal spectra of the FS [34].

We have also studied the P dependence of the spherical part of the FS of lithium. Under compression, as the FS becomes larger, a shift to higher frequencies is expected. High P experiments were done in a nonmagnetic miniature turnbuckle diamond anvil cell (DAC) [50], small enough to fully rotate in the constrained dimensions of a high field magnet bore. The composite gaskets used were MP35N formers with an insert of diamond powder and epoxy. Inside the P chamber, the sample was placed in a three-turn TDO coil of 150-μm inner diameter, made of 12-μm diameter insulated copper wire. Mineral oil was used as a P-transmitting medium.

High P data were collected in ^{3}He magnets at a base temperature of 360 mK. Data from the 18 T superconducting magnet were analyzed in the 16–18-T range and from the 35-T resistive magnet in the 28–30-T range. The P was measured using ruby fluorescence both at room and base temperatures with a fiber optic collecting system. We observe a P-induced shift of the frequency spectrum to higher values between 0 and 2.8 GPa [Fig. 2(a)]. In contrast to ambient P data, the peaks at higher pressures are concentrated in a small frequency range. However, it is possible that due to the lower signal to noise ratio in high P experiments, we were unable to detect the weaker peaks. The P dependence and value of the highest amplitude peaks are consistent with theoretically calculated values for fcc [Figs. 2(b) and 2(d)]. The comparison indicates that the fraction of fcc increases with P. We also succeeded to measure the FS of ^{7}Li at higher pressures (Fig. S12 of the Supplemental Material [48]). The P was determined to be 4.7 GPa at room temperature, however, we were unable to measure P at low temperature due to technical difficulties. Since we expect a P increase during cooling, the low temperature P was estimated the by extrapolation of the fcc data [46]. The peak position in this experiment is 51.4 kT, for which we estimate the low temperature P to be $\sim$9 GPa. At the highest P, nonhydrostatic conditions led to phase smearing which significantly reduced the amplitude of QO. Observation of QO at higher P requires modifications to the design of the current DAC to allow loading of helium or other quasihydrostatic P medium.

We measured its electron effective mass (m^*) at 1.7 GPa from the temperature dependencies of the QO amplitudes (Fig. 3). The temperature reduction factor of the amplitude (R_T) is given by $R_T = (\frac{2\pi^2 pkT}{\beta^* H})/\sinh(\frac{2\pi^2 pkT}{\beta^* H})$, where, $p = 1$ for the first harmonic term, $\beta^* = \frac{eh}{2\pi m^* c}$, e is the electron charge, h is the Planck constant, c is speed of light, H is the magnetic field, k is the Boltzmann constant, and T is the temperature. Fitting this equation with our temperature dependent data at 1.7 GPa results in $m^* = 2.30 \pm 0.15 m_0$. Where m_0 is the free electron mass. The previously reported m^* at ambient P is $(2.10 \pm 0.06) m_0$ [27].

We have calculated the band mass m_b associated with each extreme orbit on the FS of lithium [Fig. 3(c)–3(e) and Table S1 of the Supplemental Material [48]] and the principal SdH peaks for Na (Table S2). Assuming that the difference between the measured m^* and calculated m_b is entirely due

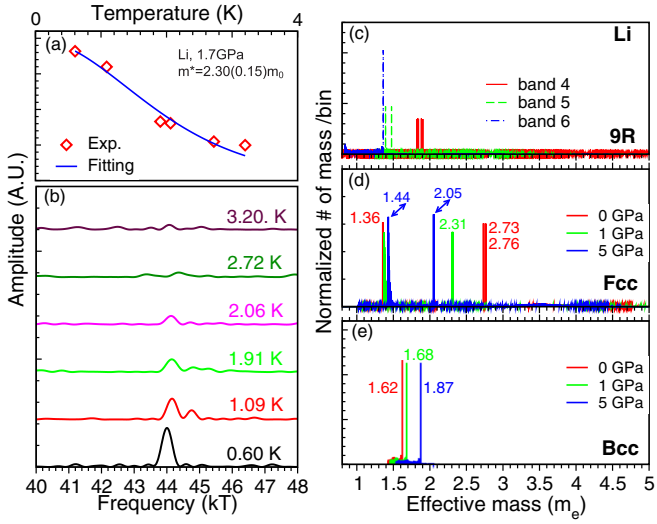

FIG. 3. (a) Amplitude of the SdH peaks vs T at 1.7 GPa. A fit using the expression for R_T gives electron effective mass of $2.30 \pm 0.15 m_0$. (b) SdH frequency spectrum of ^{7}Li at 1.7 GPa at different temperatures. At 1.09 K the main peak is split into two and the intensity of the peaks are added. (c)–(e) Theoretical calculations of band mass (m_b) of Li in the (c) 9R, (d) fcc, and (e) bcc structures at selected pressures for fcc and bcc, and at 0 GPa for 9R. The plots show histograms of m_b calculated for all angular orientations (corresponding to all extreme orbits) and grouped in bins with size equal to $10^{-4} m_e$. All orientations are sampled by varying the angles ϕ and θ from 0 to 90° and 0 to 360°, respectively, in increments of 1°. The definitions of ϕ and θ are as in Fig. 6(D) of Ref. [46]. The band masses of the electrons in the principal orbits of bcc and fcc at the selected P are given in the plot with different colors. For 9R the colors distinguish m_b originating from different bands; the 9R band structure is shown in SI Appendix [46], Fig. S5, of Ref. [46]. For all structures, the lower m_b values are for orbits along the spherical part of the FS, while the neck orbits have higher m_b. The former increase with P, while the latter decrease.

to electron-phonon effects, the two are related via $m^* = m_b(1 + \lambda)$, where λ is the electron-phonon coupling constant, which was previously estimated [20] to be 0.51 in bcc Li and 0.41 in 9R. The spherical parts of the FS represent nearly free electron states and the corresponding m_b are closer to unity. Accordingly, m_b is smaller in Na than in Li in both bcc and fcc, and slightly smaller for bcc-Na than fcc-Na. Overall, there is a weak P dependence for m_b in Na. This is consistent with previous calculations [51] which reported a slight increase in m^* from $1.031 m_0$ to $1.036 m_0$ when Na is compressed from 0 to 0.4 GPa; our values for bcc Na at 0 GPa are $1.0367 m_0$ (average) and $1.0355 m_0$ (principal peak). Notice that Elliott and Datars [37] reported slightly decreasing m^* in Na from 0 to 0.35 GPa. However, the slope of their measured m^* versus P is small compared to the experimental uncertainties.

The FS of Li has more spherical deformation than that of Na in all structures. Therefore, even in bcc-Li m_b (and m^*) is higher than in bcc-Na and exhibits stronger P dependence. Furthermore, the FS in fcc-Li has necks and the SdH orbits passing through them have significantly higher m^* than those from the spherical region of the FS. The P dependence of m_b of these orbits is also stronger, but opposite; m_b decreases with P. Since in the high-P experiment, we are only focusing on the spherical part of the FS, the actual value of m_b for the electrons in neck orbits is not relevant for the purpose of direct comparison. However, the presence of neck orbits is at least partially reflected by the measurements. The interaction of the FS with the BZ boundaries causes deformation of the belly region of the FS as well. The effect is twofold. On one hand, the volume of the spherical region decreases, thus making the electron states within this region more free electron like. This is the reason why the principal orbits of fcc-Li have smaller m_b than that of bcc-Li [see Fig. 3(c)]. On the other hand, the fraction of belly orbits which pass near the neck regions and acquire higher effective mass increases. Theoretically, in bulk Li there is a partial cancellation of the P dependence of m_b from the spherical and neck regions of the FS. As a result, the weighted average m_b (Table S1 [48]) initially increases with P until about 1 GPa, after which it begins to decrease slowly, but remains higher than that of bcc-Li and Na (bcc and fcc).

Comparison of the calculated m_b with the experimental m^* for orbits near 42 kT for different candidate structures of Li supports the model that Li consists of more than one structure and that a mixture for two or more phases (bcc, fcc, and possibly 9R) is present in the sample; for fcc alone we have $m_b(1 + \lambda) < 2.11 m_0$ at 1.7 GPa, which is lower than the experimental $m^* = 2.30 \pm 0.15 m_0$. The observed changes in the effective mass with P are the combined effect of (1) the P dependence of m^* of different structures with orbits near 42 kT, and (2) the relative stability of these phases as a function of P (and temperature). Notably, the martensitic transition is monotonically suppressed in Na, while enhanced by external P up to 3 GPa in Li. Therefore, Li has larger m^*, increasing under compression, with a stronger P dependence compared to Na.

In summary, we present a high-resolution study of the spherical part of the FS of isotopically pure ^{7}Li. By using large single grain polycrystalline samples in high magnetic fields, we establish that the principal peak of the FS of lithium at ambient P is made up of three distinct peaks. Based on comparative calibrations against sodium and comparison with theoretical calculations [46], we propose that these peaks originate from distinct crystal structures. The locations of the peaks are consistent with contributions from bcc and fcc domains, with a larger contribution from the fcc structure. This is compatible with previous results from molecular dynamics simulations on the proposed structures of lithium martensite. These data can be used in calculations of the ambient P superconductivity of lithium. We also present the measurements of the FS of lithium for pressures above 4.7 GPa in the fcc region and directly measure the changes in the size of the spherical part of its FS under compression. The electron effective mass measurements at 1.7 GPa show that lithium remains a nearly free electron system under compression. Although the present measurements were limited below the onset of high-P superconductivity and predicted topological states of lithium, they demonstrate the essential steps towards the extension of these studies to higher pressures.

The authors acknowledge the major contributions, theoretical support, supervision, and discussions during this project by N. W. Ashcroft who unfortunately passed away prior to

writing the manuscript. The authors acknowledge guidance and support from R. Hoffman throughout this project. We thank L. Adams for help with data analysis. The experimental research at University of Utah was supported by National Science Foundation Division of Materials Research Awards No. 13519862 and No. 2132692 and the U.S. Department of Energy, Office of Science, Fusion Energy Sciences under Award No. DE-SC0020340. The work at Guelph was funded by Natural Sciences and Engineering Research Council of Canada (Grant No. RGPIN-2017-03931) (E.J.N.). The theoretical research was enabled in part by support provided by Graham & Cedar and Compute Canada [52]. The work at KFUPM was supported by the Deanship of Scientific Research through Project No. SR211002. The work at LLNL was performed under the auspices of the U.S. Department of Energy under Contract No. DE-AC52-07NA27344. The National High Magnetic Field Laboratory is supported by the National Science Foundation through NSF/DMR-1157490/1644779 and the State of Florida. The work at NHMFL was also partially funded by the U.S. DOE under Grant No. NNSA SSAA DENA0001979.

S.F.E. performed the theoretical calculations. S.A.B. and E.J.N. supervised the theoretical research. A.D.G., W.A.C., and S.W.T. provided user support for the magnet time. Experimental data collection, analysis, and sample preparation were performed by T.B., A.D.G., W.C., M.T.H., and S.D. S.D. designed and supervised the experiments. All authors contributed to the writing of the paper.

[1] B. T. Matthias, Empirical relation between superconductivity and the number of valence electrons per atom, Phys. Rev. **97**, 74 (1955).

[2] J. Tuoriniemi, K. Juntunen-Nurmilaukas, J. Uusvuori, E. Pentti, A. Salmela, and A. Sebedash, Superconductivity in lithium below 0.4 millikelvin at ambient pressure, Nature (London) **447**, 187 (2007).

[3] C. L. Guillaume, E. Gregoryanz, O. Degtyareva, M. I. McMahon, M. Hanfland, S. Evans, M. Guthrie, S. V. Sinogeikin, and H. K. Mao, Cold melting and solid structures of dense lithium, Nat. Phys. **7**, 211 (2011).

[4] F. A. Gorelli, S. F. Elatresh, C. L. Guillaume, M. Marqués, G. J. Ackland, M. Santoro, S. A. Bonev, and E. Gregoryanz, Lattice Dynamics of Dense Lithium, Phys. Rev. Lett. **108**, 055501 (2012).

[5] M. Hanfland, K. Syassen, N. E. Christensen, and D. L. Novikov, New high-pressure phases of lithium, Nature (London) **408**, 174 (2000).

[6] J. B. Neaton and N. W. Ashcroft, Pairing in dense lithium, Nature (London) **400**, 141 (1999).

[7] S. F. Elatresh, Z. Zhou, N. W. Ashcroft, S. A. Bonev, J. Feng, and R. Hoffmann, High-Pressure lithium as an elemental topological semimetal, Phys. Rev. Materials **3**, 044203 (2019).

[8] S. A. Mack, S. M. Griffin, and J. B. Neaton, Emergence of topological electronic phases in elemental lithium under pressure, Proc. Natl. Acad. Sci. USA **116**, 9197 (2019).

[9] Z. Yu, H. Y. Geng, Y. Sun, and Y. Chen, Optical properties of dense lithium in electride phases by first-principles calculations, Sci. Rep. **8**, 3868 (2018).

[10] A. M. Schaeffer, S. R. Temple, J. K. Bishop, and S. Deemyad, High-Pressure superconducting phase diagram of ^{6}Li: Isotope effects in dense lithium, Proc. Natl. Acad. Sci. USA **112**, 60 (2015).

[11] K. Shimizu, H. Ishikawa, D. Takao, T. Yagi, and K. Amaya, Superconductivity in compressed lithium at 20 K, Nature (London) **419**, 597 (2002).

[12] V. V. Struzhkin, M. I. Eremets, W. Gan, H. Mao, and R. J. Hemley, Superconductivity in dense lithium, Science **298**, 1213 (2002).

[13] S. Deemyad and J. S. Schilling, Superconducting Phase Diagram of Li Metal in Nearly Hydrostatic Pressures Up to 67 GPa, Phys. Rev. Lett. **91**, 167001 (2003).

[14] N. E. Christensen and D. L. Novikov, Calculated superconductive properties of Li and Na under pressure, Phys. Rev. B **73**, 224508 (2006).

[15] N. E. Christensen and D. L. Novikov, Predicted Superconductive Properties of Lithium Under Pressure, Phys. Rev. Lett. **86**, 1861 (2001).

[16] T. Bazhirov, J. Noffsinger, and M. L. Cohen, Electron-Phonon coupling in bcc lithium, Phys. Rev. B **84**, 125122 (2011).

[17] K. Iyakutti and C. N. Louis, High-Pressure band structure and superconductivity of bcc and fcc lithium, Phys. Rev. B **70**, 132504 (2004).

[18] A. Rodriguez-Prieto, A. Bergara, V. M. Silkin, and P. M. Echenique, Complexity and Fermi surface deformation in compressed lithium, Phys. Rev. B **74**, 172104 (2006).

[19] C. F. Richardson and N. W. Ashcroft, Effective electron-electron interactions and the theory of superconductivity, Phys. Rev. B **55**, 15130 (1997).

[20] A. Y. Liu and M. L. Cohen, Electron-Phonon coupling in bcc and 9R lithium, Phys. Rev. B **44**, 9678 (1991).

[21] A. Rodriguez-Prieto and A. Bergara, Fermi surface deformation in lithium under high pressure, High Press. Res. **26**, 461 (2006).

[22] D. Kasinathan, J. Kuneš, A. Lazicki, H. Rosner, C. S. Yoo, R. T. Scalettar, and W. E. Pickett, Superconductivity and Lattice Instability in Compressed Lithium from Fermi Surface Hot Spots, Phys. Rev. Lett. **96**, 047004 (2006).

[23] D. Graf, R. Stillwell, T. P. Murphy, J. H. Park, M. Kano, E. C. Palm, P. Schlottmann, J. Bourg, K. N. Collar, J. Cooley, J. Lashley, J. Willit, and S. W. Tozer, Fermi surface of alpha uranium at ambient pressure, Phys. Rev. B **80**, 241101(R) (2009).

[24] D. Graf, R. Stillwell, T. P. Murphy, J. H. Park, E. C. Palm, P. Schlottmann, R. D. McDonald, J. G. Analytis, I. R. Fisher, and S. W. Tozer, Pressure dependence of the $BaFe_2As_2$ Fermi surface within the spin density wave state, Phys. Rev. B **85**, 134503 (2012).

[25] J.-P. Jan, W. B. Pearson, and Y. Saito, De Haas-van Alphen Effect and Fermi Surface of Ordered Alloys of the Beta Brass Type, Proc. R. Soc. London, Ser. A **297**, 275 (1967).

[26] P. A. Goddard, J. Singleton, R. D. McDonald, N. Harrison, J. C. Lashley, H. Harima, and M. T. Suzuki, Catastrophic Fermi Surface Reconstruction in the Shape-Memory Alloy AuZn, Phys. Rev. Lett. **94**, 116401 (2005).

[27] S. Hashimoto, T. Yasuda, T. Kubo, H. Shishido, T. Ueda, R. Settai, T. D. Matsuda, Y. Haga, H. Harima, and Y. Ōnuki, The de Haas–van Alphen effect and the Fermi surface in $CePt_3$ Si and $LaPt_3$ Si, J. Phys.: Condens. Matter **16**, L287 (2004).

[28] N. Kimura, T. Komatsubara, D. Aoki, Y. Onuki, Y. Haga, E. Yamamoto, H. Aoki, and H. Harima, Observation of a main Fermi surface in UPt_3, J. Phys. Soc. Jpn. **67**, 2185 (1998).

[29] A. J. Arko and J. E. Schirber, Fermi surface measurements in actinide metals and compounds, J. Phys. Colloq. **40**, C4-9 (1979).

[30] C.-H. Li, Y.-J. Long, L.-X. Zhao, L. Shan, Z.-A. Ren, J.-Z. Zhao, H.-M. Weng, X. Dai, Z. Fang, C. Ren, and G. F. Chen, Pressure-Induced topological phase transitions and strongly anisotropic magnetoresistance in bulk black phosphorus, Phys. Rev. B **95**, 125417 (2017).

[31] T. Ideue, M. Hirayama, H. Taiko, T. Takahashi, M. Murase, T. Miyake, S. Murakami, T. Sasagawa, and Y. Iwasa, Pressure-Induced topological phase transition in noncentrosymmetric elemental tellurium, Proc. Natl. Acad. Sci. USA **116**, 25530 (2019).

[32] D. L. Randles and M. Springford, Observation of de Haas-van Alphen oscillations in a lithium dispersion, J. Phys. F: Met. Phys. **3**, L185 (1973).

[33] D. L. Randles and M. Springford, De Haas-van Alphen effect in alkali metal dispersions and the Fermi surface of lithium, J. Phys. F: Met. Phys. **6**, 1827 (1976).

[34] M. B. Hunt, P. H. P. Reinders, and M. Springford, a de Haas-van Alphen effect study of the Fermi surface of lithium, J. Phys.: Condens. Matter **1**, 6589 (1989).

[35] J. J. Donaghy and A. T. Stewart, Fermi surface of lithium by positron annihilation, Phys. Rev. **164**, 391 (1967).

[36] D. Shoenberg, *Magnetic Oscillations in Metals* (Cambridge University Press, Cambridge, England, 1984).

[37] M. Elliott and W. R. Datars, De Haas-van Alphen effect in sodium under pressure, J. Phys. F: Met. Phys. **12**, 465 (1982).

[38] W. A. Coniglio, L. E. Winter, C. Rea, K. Cho, and C. C. Agosta, Improvements to the Tunnel Diode Oscillator Technique for High Frequencies and Pulsed Magnetic Fields with Digital Acquisition, arXiv:1003.5233.

[39] H. Kim, M. A. Tanatar, and R. Prozorov, Tunnel diode resonator for precision magnetic susceptibility measurements in a MK temperature range and large DC magnetic fields, Rev. Sci. Instrum. **89**, 094704 (2018).

[40] S. F. Elatresh, M. T. Hossain, T. Bhowmick, A. D. Grockowiak, W. Cai, W. A. Coniglio, S. W. Tozer, N. W. Ashcroft, S. A. Bonev, S. Deemyad, and R. Hoffmann, Fermi surface studies of the low-temperature structure of sodium, Phys. Rev. B **101**, 220103(R) (2020).

[41] M. J. G. Lee, The de Haas–van Alphen effect and the Fermi surface of sodium, Proc. R. Soc. Lond. A **295**, 440 (1966).

[42] A. W. Overhauser, Crystal Structure of Lithium at 4.2 K, Phys. Rev. Lett. **53**, 64 (1984).

[43] R. Berliner, O. Fajen, H. G. Smith, and R. L. Hitterman, Neutron powder-diffraction studies of Lithium, Sodium, and potassium metal, Phys. Rev. B **40**, 12086 (1989).

[44] R. Berliner, H. G. Smith, J. R. D. Copley, and J. Trivisonno, Structures of sodium metal, Phys. Rev. B **46**, 14436 (1992).

[45] H. Abe, K. Ohshima, T. Suzuki, S. Hoshino, and K. Kakurai, Neutron-Scattering study of metallic sodium, Phys. Rev. B **49**, 3739 (1994).

[46] S. F. Elatresh, W. Cai, N. W. Ashcroft, R. Hoffmann, S. Deemyad, and S. A. Bonev, Evidence from Fermi surface analysis for the low-temperature structure of lithium, Proc. Natl. Acad. Sci. USA **114**, 5389 (2017).

[47] G. J. Ackland, M. Dunuwille, M. Martinez-Canales, I. Loa, R. Zhang, S. Sinogeikin, W. Cai, and S. Deemyad, Quantum and isotope effects in lithium metal, Science **356**, 1254 (2017).

[48] See Supplemental Material at http://link.aps.org/supplemental/10.1103/PhysRevB.106.L041112 for theoretical and experimental data analysis.

[49] M. Rasolt, S. B. Nickerson, and S. H. Vosko, Non-Local exchange and correlation effects on the Fermi surface of lithium, Solid State Commun. **16**, 827 (1975).

[50] D. E. Graf, R. L. Stillwell, K. M. Purcell, and S. W. Tozer, Non-metallic gasket and miniature plastic turnbuckle diamond anvil cell for pulsed magnetic field studies at cryogenic temperatures, High Press. Res. **31**, 533 (2011).

[51] L. Wilk, A. H. MacDonald, and S. H. Vosko, Calculations of the spin susceptibilities and their volume dependence for Li, Na, and k, Can. J. Phys. **57**, 1065 (1979).

[52] www.computecanada.ca.